Bioprocess and Biosystems Engineering
https://doi.org/10.1007/s00449-021-02609-4

RESEARCH PAPER

Novel dual-flow perfusion bioreactor for in vitro pre-screening of nanoparticles delivery: design, characterization and testing

Maria Elena Lombardo[1,2] · Francesco Carfì Pavia[1,5] · Emanuela Fabiola Craparo[3] · Elisa Capuana[1] · Gennara Cavallaro[3,4] · Valerio Brucato[1] · Vincenzo La Carrubba[1,4]

Received: 20 April 2021 / Accepted: 26 June 2021

Abstract

An advanced dual-flow perfusion bioreactor with a simple and compact design was developed and evaluated as a potential apparatus to reduce the gap between animal testing and drug administration to human subjects in clinical trials. All the experimental tests were carried out using an ad hoc Poly Lactic Acid (PLLA) scaffold synthesized via Thermally Induced Phase Separation (TIPS). The bioreactor shows a tunable radial flow throughout the microporous matrix of the scaffold. The radial perfusion was quantified both with permeability tests and with a mathematical model, applying a combination of Darcy's Theory, Bernoulli's Equation, and Poiseuille's Law. Finally, a diffusion test allowed to investigate the efficacy of the radial flow using Polymeric Fluorescent Nanoparticles (FNPs) mimicking drug/colloidal carriers. These tests confirmed the ability of our bioreactor to create a uniform distribution of particles inside porous matrices. All the findings candidate our system as a potential tool for drug pre-screening testing with a cost and time reduction over animal models.

Keywords Dual-flow perfusion bioreactor · 3D Scaffold · Fluid dynamics · Tunable radial flow · Polymeric fluorescent nanoparticles

Introduction

The development of a novel drug is a time-consuming and costly process including several stages [1]. Currently, the estimated costs for a successful clinical product exceed US $1 billion with development timelines over 12 years, of which pre-clinical in vitro testing consuming around half of the total [2]. The costs of failure are considerable and involve diverse non-scientific factors together with scientific and technological contributions [3]. The choice of appropriate pre-clinical models has a paramount importance to increase the possibilities of successfully completing a clinical trial [2]. Traditionally, drug screening methods include in vivo animal experiments and in vitro cell-based screening assays [4]. The use of animals as models for human anatomy and pharmacology dates back millennia [5]. Due to practical and ethical concerns related to human experimentation, the importance of animal experimentation in future development in life science cannot be ignored [6]. However, animal models are limited in their ability to mimic the extremely complex biological in vivo environment [7]. Therefore, the use of in vitro platforms became more common as an alternative to animal experiments due to the obvious ethical, economical and scientific advantages over *in vivo* models [8]. Commonly, 2D in vitro models were used within pharmaceutical research to investigate drug metabolism and pharmacokinetic properties of absorption, distribution and excretion for new chemical entities (NCEs) [9]. Nevertheless, this assay encounters the conventional problems of static culture and, consequently, limitations related to the different cell shape, biochemical features, cellular

✉ Maria Elena Lombardo
mariaelena.lombardo01@unipa.it

1 Dipartimento di Ingegneria, University of Palermo, Viale delle Scienze building 8, 90128 Palermo, Italy

2 Centre Énergie, Matériaux et Télécommunications, Institut National de la Recherche Scientifique, 1650 Boulevard Lionel-Boulet, Varennes, QC J3X 1S2, Canada

3 Dipartimento di Scienze e Tecnologie Biologiche, Chimiche e Farmaceutiche, University of Palermo, Viale delle Scienze building 16, 90128 Palermo, Italy

4 ATeN center, University of Palermo, Viale delle Scienze building 18, 90128 Palermo, Italy

5 Consorzio Universitario di Caltanissetta, Corso Vittorio Emanuele 92, 93100 Caltanissetta, Italy

Published online: 25 July 2021

environment and cell morphology [10], which may affect cellular response to drugs. This presumably explains why many drugs pre-clinically evaluated to be "active", using 2D-cultured cell line-based models, then were proved to be clinically useless [11]. All these limitations have promoted, in the last decade, the development of three-dimensional (3D) cell culture systems that are more realistic and sophisticated models for mimicking in vivo microenvironment, in terms of control of concentration gradients of signaling molecules and therapeutic agents, composition and structure of Extra-Cellular Matrix (ECM) around the cells, as well as morphology and arrangement of individual cells [12]. Recently, Tissue engineering (TE) introduced the use of 3D support systems (called scaffolds) to provide chemical and physical support for cell growth allowing tissue-specific differentiation for regenerating human tissues [13]. Scaffold-based approaches were used to prepare many different models [14–17]. However, such static cultures do not accurately represent a natural in vivo environment for cells, due to many limitations, particularly in terms of distribution of nutrients and oxygen as well as removal of waste products [18]. This affects the signal transduction from the outside to the inside of cells, and influences gene expression and cellular behaviors such as sensitivity levels to different drugs [19]. One way to overcome these constraints has been proposed by TE with introducing bioreactors systems to control the culture environment [20]. They have the potential to mimic the complex in vivo environment in an in vitro setting, so they can be used to investigate specific biological, chemical or physical effects [21] on cellular differentiation and tissue development [22] and, consequently, to evaluate the potential of a novel drug [23] or innovative biological molecules approaches, such as siRNA [24]. Among the variety of bioreactors developed for supporting engineered tissue constructs [25, 26], the flow perfusion bioreactors are gradually gaining more interest due to their advantages, such as increasing the exchange of nutrients through the 3D scaffolds, improving the removal of waste products [27], as well as applying mechanical stress and/or electromagnetic stimuli to the cultured cells [28]. Based on the idea of improving the research for drug delivery and pre-screening tests, the use of a tubular perfusion bioreactor mimicking a blood vessel, was investigated by Al-Attar et al. [29] to understand the effect of fluid flow on the release profile of resveratrol encapsulated into electrospun microfibers. Their model showed how different operating parameters such as inlet fluid velocity, bioreactor length and cellular uptake rate can positively affect the drug release from a porous tissue-like microenvironment. Marrella et al. [30] developed an electromagnetic bioreactor device integrated with a fluidic flow system to study the drug release from biocompatible superparamagnetic Fe-hydroxyapatite NPs (FeHAs). They proved that FeHAs can be used as functional cardio-compatible nano-carriers under fluid-flow conditions resembling those of the cardiovascular environment. The possibility to have a precise measure and control of the in vitro physiological environment applying both mechanical, chemical and electrical stimuli that a cell maybe can be exposed in vivo [31], make using bioreactors and 3D dynamic culture a guarantee for providing more reliable results in terms of predicting human diseases and drug response in comparison with the traditional 2D in vitro cell culture combined with animal in vivo testing.

In this contest, together with 3D dynamic cell culture, another significant area of study within the pharmaceutical-nanotechnology industry became the evaluation of potential in drug delivery efficiency of novel nanoparticle-based drug carriers [32]. The last represent a valuable tool for pursuing the main goals of nanomedicine, such as stability, controlled release, targeted delivery and reduced toxic and side effects of entrapped drugs, to improve the treatment of a wide range of diseases [33–35]. Recently, Afshar et al. [36] fabricated and characterized sodium alginate (SA)/polyvinyl alcohol (PVA) hydrogel containing Rosuvastatin-loaded chitosan (CS) nanoparticles as a drug delivery system. From their findings, the chitosan nanoparticles had a significant effect on the drug release behavior, thanks to their homogeneous dispersion, low water solubility, and optimal mechanical properties.

The present study introduces an innovative dual-flow perfusion bioreactor used to simulate the diffusion of drug carrier models from a blood-like flow within a polymeric microporous structure.

Our apparatus allows us to control two different perfusion circuits through a porous, biocompatible Poly-L-Lactic acid (PLLA) scaffold produced via Thermally Induced Phase Separation (TIPS) [37]. The fluid-dynamic properties of the bioreactor were evaluated and the perfusion efficacy was tested qualitatively using toluidine blue as dye, and, then implementing a simple semi-empirical procedure to estimate the 3D scaffold permeability. Polymeric fluorescent nanoparticles (FNPs) based on a fluorescent polyaspartamide-polylactide graft copolymer were synthesized [38, 39] and use as drug carrier model. The transport, adhesion and distribution on blood flow of similar particles were previously evaluated to elucidate the FNPs transport toward the vessel vasculature in micro-capillary flow [40]. Here, FNPs were utilized to understand the contribution of the bioreactor perfusion flow to the mobility and distribution of particles inside polymeric scaffolds. All the obtained results demonstrate the potential of our dual-flow perfusion bioreactor as an innovative 3D in vitro model for multiple applications including TE, human therapy and drug pre-screening tests, reducing cost/time-consuming and ethical concerns related to the abused in vivo animal models.

Materials and methods

3D polymeric scaffold synthesis and characterization

For the implementation of the perfusion bioreactor, a specific hollow cylindrical scaffold was realized. The desired shape was obtained through an ad hoc created sample holder (Fig. 1i). It consists of an empty aluminium cylinder with an outside diameter (OD) of 3.5 cm and height (*H*) of 4 cm, with a cover that perfectly closes off the system, thus preventing the communication between the inside and the outside environment. Both the base of the central hole cavity [internal diameter (ID) = 2.8 cm, *H* = 1.8 cm] and the cover incorporate a 0.2 cm hole, which allows to fix a stainless-steel rod used for creating an inner channel (lumen) in the scaffold. The porous matrix was obtained via TIPS by following a one-step protocol, as adopted in a previous work [41]. Briefly, a homogeneous solution of PLLA (RESOMER L 209 S), 1–4 dioxane (Merck KGaA, Darmstadt, Germany) and deionized water was prepared using a constant dioxane-to-water weight ratio of 87:13 and a PLLA concentration of 4% (wt/wt). The homogeneous solution was initially kept at 60 °C and then poured into the sample holder. Thereafter, the temperature of the solution was suddenly lowered by pool immersion of the sample holder into a thermostatic water bath, to induce the phase separation. A temperature of 0 °C (demixing temperature) was kept for 10 min (demixing time). After a quench by immersion in an ethyl alcohol bath at − 20 °C for 15 min, the support was gently pulled out from the structure. The resulted scaffold was rinsed in deionized water and dried at 35 °C under vacuum overnight, to completely remove any solvent trace. Morphological analysis of the as-prepared scaffolds was carried out with a Scanning Electron Microscope (Phenom Pro-X, Phenom-World, Netherlands) operating at an accelerating voltage of 10 kV. The samples were kindly cut crosswise with a surgical scalpel to obtain smallest pieces with a thickness of around 0.5 cm. Then, they were mounted on a metal stub using a sticky carbon disc and finally coated with gold (thickness ~ 4 nm) in a sputter coater under argon atmosphere for increasing the conductivity. The average pore size was determined by image analysis on the SEM micrographs using Image-J software.

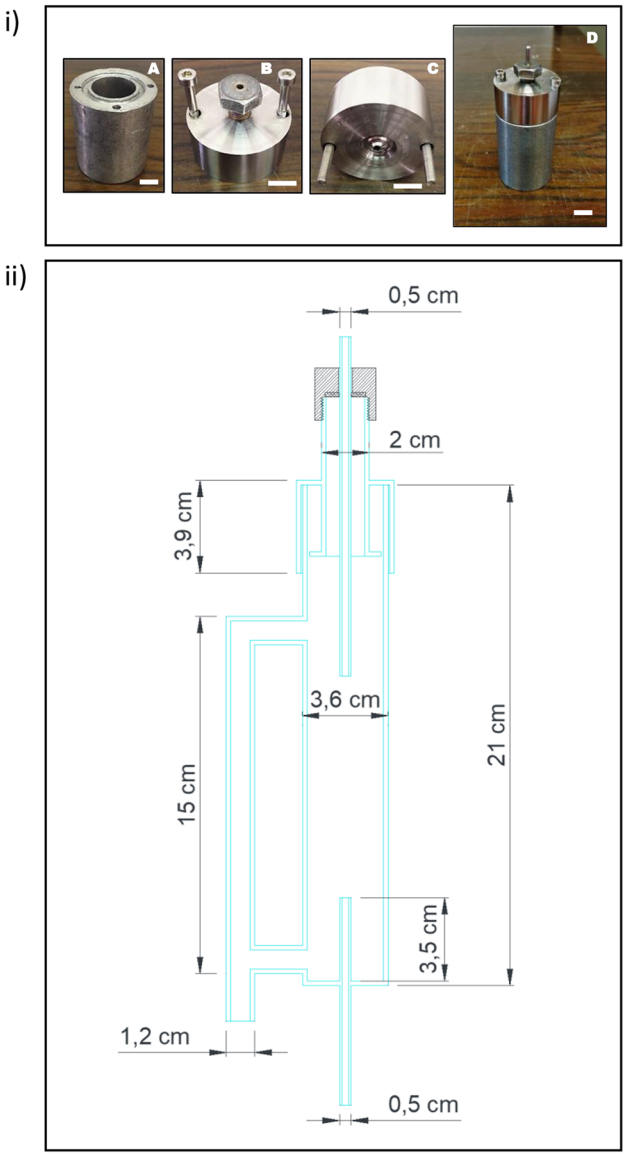

Fig. 1 **i** Aluminum sample holder for hollow cylindrical scaffold synthesis via TIPS: body (**A**), cover top view (**B**), cover bottom view (**C**); sample holder assembled (**D**). Scale bar 1 cm (**ii**) Scheme of the dual-flow bioreactor design

Bioreactor design

In this study, a dual-flow perfusion bioreactor, previously designed and built by our research group [42], was improved and characterized. It consists of two glass cylindrical tubes (a main column and a bubble column) connected to each other. As shown in Fig. 1ii, the main column has an ID of 3.6 cm and *H* of 21 cm. At the base of the column is located a glass tube (ID = 0.5 cm and *H* = 3.5 cm), which allows to fix the bottom of the scaffold. The lid of the column is characterized by a singular configuration: to block the upper part of the scaffold, the lid presents a central hole through which a thin glass tube (ID = 0.5 cm) is inserted. The distance between the upper and lower glass tubes can be adapted to accommodate scaffolds with different heights. The bubble column is a smaller glass tube (ID = 1.2 cm and *H* = 15 cm) that is connected to the main one and works as a conventional bubble column (Fig. 1ii).

Bioreactor set-up

The unique configuration of the bioreactor allows a separate control of two perfusion flows: the Internal Perfusion Circuit (IPC) and the External Perfusion Circuit (EPC). The IPC (Fig. 2i left) is integrated in the main column that works as culture chamber and where the hollow cylindrical scaffold is located. To connect the scaffold to the glass tubes, standard biocompatible polypropylene Luer-Lock connectors (Kiyatec) with 0.15 cm ID tubing were used. The medium is pumped inside the lumen, from top to bottom, by a syringe pump (New Era Single Syringe Pump NE-1000) at infusion rates from 0.73 µl/hr to 2100 ml/hr and with a dispensing accuracy of +/− 1%. The bubble column is the key component of the EPC (Fig. 2i right). It is connected to the main column and to a peristaltic pump (Model M025; VerderFlex) by means a silicone tube (ID = 0.2 cm). The air bubbles rise through the column, and drag part of the liquid to the main column, thus allowing a recirculation of the medium. In addition, the gas phase that is bubbled vertically through the liquid phase promotes the gas–liquid mass transfer, as in a conventional bubble column [43], thus improving the oxygenation of the medium. During operation, the whole system can be placed in a standard cell culture incubator at 37 °C in a humidified atmosphere of 95% air and 5% CO_2 to maintain constant operating conditions.

EPC flow analysis

Upon completion of the device construction, evaluation of bioreactor fluid dynamics was carried out. An EPC flow analysis was assessed to accurately control the air and liquid flow rates simply by varying the RPM of the pump. For measuring the air flow rate, a bubble soap flowmeter was employed (Fig. 2ii). The bioreactor was connected to a volumetric glass tube containing a small amount of liquid soap. As the peristaltic pump draws air through the system, a flat soap bubble is interposed in the flow path. In

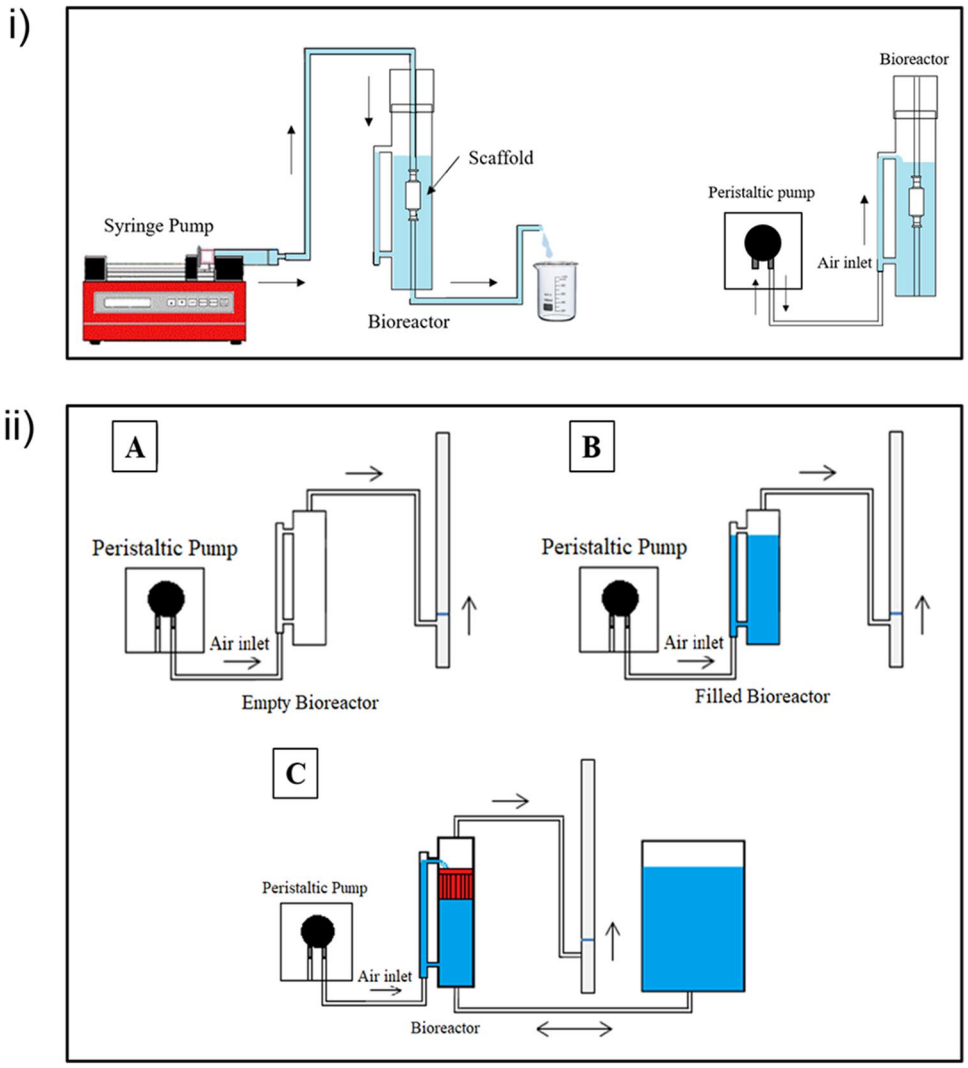

Fig. 2 **i** Scheme of the Inner Perfusion Circuit (IPC) (left) and the Externa Perfusion Circuit (right). **ii** Set-up used for the air flow rate investigation, with both empty (**A**) and filled bioreactor (**B**), and for the liquid flow rate analysis (**C**)

principle, while the air flow causes the soap film to move from one volume mark to another, the travel time is measured with a stopwatch. The flow rate can then be directly calculated using the travel time and the known tube volume. Here, we measured the distance covered by the rising bubble generated by the water soap solution after 1 min, and consequently, we were able to determine the air volume. A wide range of RPM for the peristaltic pump was evaluated (from 27 to 110). This analysis was conducted for both empty (Fig. 2ii A) and liquid-filled (Fig. 2ii B) bioreactor. Moreover, the volume of liquid dragged by the rising air bubbles in the bubble column was also evaluated. For this testing, the main column was connected to a larger diameter reservoir to keep constant the liquid level of the column during the measurements (Fig. 2ii C). The liquid volume dragged in 1 min was collected in a silicone box and measured by weighting. For this evaluation, a working range between 27 and 85 RPM was investigated. The flow rates analysis of IPC was extensively discussed in a previous work [42].

Perfusion system characterization

For evaluating the efficiency of the radial perfusion through the scaffold, permeability tests were performed. A qualitative diffusion test was carried out adding toluidine blue to the deionized water (0.1% v/v) as dye to visibly observe the staining of the scaffold. Specifically, a known volume of aqueous solution (60 ml) was pumped inside the scaffold with a constant flow rate of 1 ml/min, corresponding to a superficial linear velocity of 10 mm/s. After 30 min, the cross-sections of the as-treated scaffolds were observed both macroscopically and under stereo-microscope (Euromex, Holland). The second test aimed to explore the possibility to control the radial perfusion flow, in terms of flow direction and flow rate. Deionized water at a constant flow rate (0.5 ml/min and 1 ml/min) was dispensed by a syringe pump (New Era Single Syringe Pump NE-1000) via the IPC, inside the lumen of the scaffold located into the water-filled main column. After a well-defined time, the water come out from the circuit was weighted. The radial flow across the scaffold was obtained by subtracting the mean weight of the water outflowing from the syringe pump (measured independently previously) from the mean reading of three measurements. Several tests were conducted by varying the height level between the bottom of the scaffold and the outlet of IPC tube (H), as depicted in Fig. 3. Five different levels were investigated with ΔH of 5 cm among each level.

The same data obtained from the above-described experiment were used also to estimate the permeability of the scaffold. Darcy's Law in cylindrical geometry was applied for the permeability evaluation (Eq. 1).

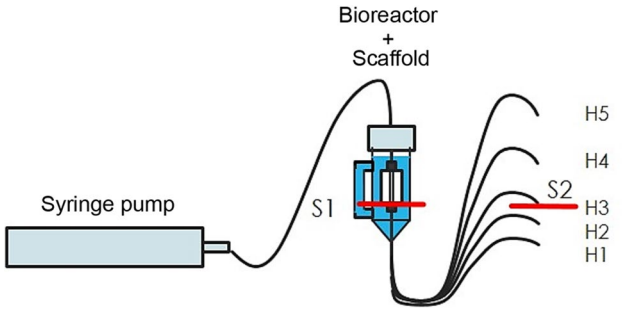

Fig. 3 Experimental apparatus for scaffold permeability evaluation. For the calculation of the pressure in the lumen of the scaffold, Bernoulli's law was applied between the level S1 and the level S2 (red solid lines)

$$Q = \frac{K\,2\,\pi\,h_s\,\left(P_{\text{ext}} - P_{\text{int}}\right)}{\mu\,\ln\frac{r_{\text{ext}}}{r_{\text{int}}}} \tag{1}$$

where Q is the radial flow, K is the permeability (m^2), h_s is the scaffold height (m), P_{ext} and P_{int} (Pa) are the pressure values at the scaffold external surface and in the lumen, respectively, μ is the fluid viscosity (Pa s), and r_{ext} and r_{int} are the external and internal radii of the scaffold (m), respectively. To calculate the permeability K, Darcy's Equation ought to be solved for a range of pressure drops across the perfused scaffold, as specified in Eq. 2:

$$K = \frac{Q}{\left(P_{\text{ext}} - P_{\text{int}}\right)} \times \frac{\mu\,\ln\frac{r_{\text{ext}}}{r_{\text{int}}}}{2\,\pi\,h_s} \tag{2}$$

where $Q/(P_{\text{ext}} - P_{\text{int}})$ is the slope of the curve that represent the permeated flow as a function of the pressure drops across the scaffold. Hence, to derive this curve, the permeated flow previously measured at different H was used, and the corresponding pressure drops across the scaffold were obtained from the hydrostatic wall pressure of the surrounding water at the scaffold base (P_{ext}), and by applying the Bernoulli's Law (Eq. 3) to determine the average pressure at the inner channel of the scaffold (P_{int}).

$$\frac{P_1}{\rho g} + \frac{v_1^2}{2g} + z_1 = \frac{P_2}{\rho g} + \frac{v_2^2}{2g} + z_2 + y_{\text{distr}} \tag{3}$$

where Pi is the pressure at the considered i-section (Pa), v_i the fluid velocity (m/s), z_i the static height (m), g the gravitational acceleration (m^2/s), ρ is the fluid density (kg/m^3), and y_{distr} the pressure drops (m). Specifically, Bernoulli's law was applied between the outlet of the IPC tube (S2), and the bottom of the scaffold (S1), as defined in Fig. 3.

If using a tube with the same diameter of the inner channel of the scaffold (2 mm), Bernoulli's equation was reduced to:

$$P_1 = P_2 + (z_2 - z_1 - y_{distr}) \times \rho g \quad (4)$$

where P_1 corresponds to P_{int}, P_2 is the atmospheric pressure (Pa), and $z_2 - z_1$ is the above-defined H. According to the evaluated Reynold's number for the applied fluid flows, y_{distr} was estimated by the Poiseuille's Law (Eq. 5), valid for Newtonian, and incompressible fluid flowing in a laminar regime.

$$y_{distr} = \frac{2fLv^2}{Dg} \quad (5)$$

where f is the friction factor (calculated as 16/Re for laminar flow regimes), L is the length of the tube, v the fluid velocity along the tube and D the tube diameter.

The obtained curve of the perfused flow rate as a function of the pressure drop across the scaffold was derived for two flow rates (0.5 ml/min and 1 ml/min), and the resulting permeability values were calculated. All the obtained data were plotted using Origin Lab Software.

Fabrication of polymeric fluorescence nanoparticles (FNPs)

α,β-Poly(N-2-hydroxyethyl)-D,L-aspartamide (PHEA) was synthesized and characterized as described previously in literature [44]. The chemical functionalization of PHEA with rhodamine B (RhB), Polylactic acid (PLA) (average molecular weight 14,000 Da) and polyethylene glycol (PEG) molecules (average molecular weight 2000 Da) was carried out by following synthetic procedures already described in literature [38, 39, 45]. Spectroscopic data were in agreement with the reported structure. The degree of functionalization, in terms of molar ratio between each reactant and repeating units was equal to 0.61% for RhB, 4% for PLA and 12.4% for PEG. FNPs were obtained using the emulsion–high pressure homogenisation (HPH) procedure [39]. Briefly, a PHEA-g-RhB-g-PLA-g-PEG graft copolymer was dispersed in dichloromethane at a concentration of 20 mg/ml (4 ml) and the obtained dispersion was used as organic phase to obtain a o/w emulsion with the aqueous phase (80 ml) by stirring at 20,500 RPM. The latter o/w emulsion was homogenized one time at 7500 psi using an EmulsiFlex TM-C5 as homogenizer (Avestin Inc.). FNPs were obtained by evaporation of the organic solvent under reduced pressure, then diluted with NaCl aqueous solution to obtain an isotonic aqueous FNPs dispersion (milli-Q water with 0.9% NaCl) at a concentration of 0.1 mg/ml. The mean number distribution diameter and ζ potential measurement of FNPs were performed using the Zetasizer Nano ZSP (Malvern Instrument) [39]. Size analyses were done on the isotonic aqueous FNPs dispersion at a concentration of 0.1 mg/ml with a fixed angle of 173° and at 25 °C.

Diffusion studying

A diffusion test was carried out to investigate the potential distribution of a fluorescent drug/colloidal carrier inside the scaffold. 40 ml of an isotonic aqueous FNPs solution at a concentration of 0.1 mg/ml were pumped in the lumen at a constant flow rate of 1 ml/min. The circulation loop was repeated three times to ensure a complete permeation of the scaffold volume and a diffusion of the solution till the external surface of the construct. Afterwards, the scaffold was extracted from the bioreactor, dried overnight and processed for further analyses. To illustrate the presence and distribution of FNPs among the polymeric matrix, different cross sections were prepared as described above and observed by SEM (Phenom ProX, Phenom-World, The Nederland, voltage 10.0 kV). Three areas were focused: lumen surface, polymeric matrix close to the lumen and polymeric matrix far from the lumen. Other dried cross sections were used for the fluorescence analysis. They were located on a standard glass microscope slide and observed with an inverted fluorescence microscope (Leica DM 2500) equipped with a charge-coupled device camera. A 530–550 nm band-pass excitation filter was selected for detecting the red emission of Rhodamine B and blocking any green emission. The fluorescence distribution was qualitatively evaluated for 4 regions (moving from the lumen to the external surface) of the polymeric matrix. Moreover, the fluorescence images were used for a quantitative analysis of the FNPs radial distribution into the scaffold by determining the fluorescence signal intensity using Image-J Software. 3 different pictures were analyzed per each region and at least 20 squares of the same area were examined for each picture. The results were expressed as mean ± standard deviation (SD). A statistical test was performed using Origin2021 and ANOVA with Tukey's correction for the comparison between different groups. A p value < 0.05 was accepted as statistical significance.

Results

Morphology and porosity of PLLA scaffold

We selected TIPS as technique for the synthesis of a hollow cylindric PLLA scaffold using an ad hoc aluminum sample holder (described in Materials and Methods section). Thin slices (thickness 0.5 cm) from different areas of the as-obtained scaffold (OD = 2.5 cm, ID = 0.2 cm, H = 3.5 cm) were analyzed to verify the homogeneity of the sample structure. The cross-section morphologies are shown in Fig. 4. SEM micrograph of the external polymeric matrix reveals an average pore size of about

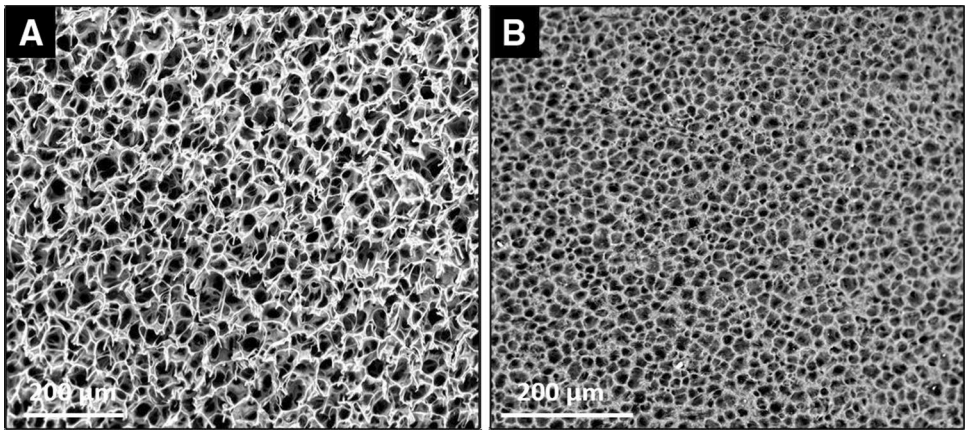

Fig. 4 SEM micrographs of PLLA scaffold produced by TIPS at 0 °C for 10 min. **A** External polymeric matrix. **B** Lumen surface in contact with the metallic support. Scale bar 200 µm

30–40 µm (Fig. 4A). The surface of the lumen was also microporous, with a pore size of 20–30 µm, as observed in Fig. 4B.

Bioreactor fluid dynamics characterization: EPC

To demonstrate the capability of controlling the airflow in a reliable and reproducible way, an experimental characterization of the system was carried out. The flow rates of the EPC were measured for both empty and filled bioreactor with a fixed volume of culture medium. The data were plotted as a function of RPM of the peristaltic pump (Fig. 5A) and showed that the flow rates did not change considerably between the two conditions. Figure 5B indicates the liquid flow rate circulating from the bubble column to the main column, thanks to the rising air bubbles, as a function of the pump speed (RPM). Comparing the two results, a direct proportion was found between the air and liquid flow rates (Fig. 5C). Together these results demonstrate the wide range of flow rate coverable with our device and underline the significant reliability of the entire system.

Efficiency of the perfusion system

As a matter of fact, perfusion is one of the tissue growth conditions that maintain cell viability thanks to continuous medium flow and nutriment supply during a dynamic cell culture [46]. Here, the radial perfusion flow through the porous scaffold was evaluated. The experiment was conducted using a wet scaffold located inside the main column pre-filled with deionized water. To evaluate the diffusion through the porous matrix, a blue dye (toluidine blue) at a concentration of 0.1% v/v was added to deionized water. After 30 min of circulation inside the bioreactor at a fixed flow rate of 1 ml/min, the scaffold was extracted and cut in different slices from the upper, center and bottom part. In Fig. 6A–C, a clear radial staining of the matrix can be appreciated. From the cross sections, it is possible to appreciate that the blue dye permeated uniformly inside the microporous structure from the lumen to the external surface of the scaffold and from top to bottom. Radial flow rates through the hollow cylindrical scaffold were measured at two different IPC flow rates (0.5 ml/min and 1 ml/min) and for different heights (*H*) (Fig. 3). Figure 7A shows the calculated radial flow rates. By convention, we assumed the flux

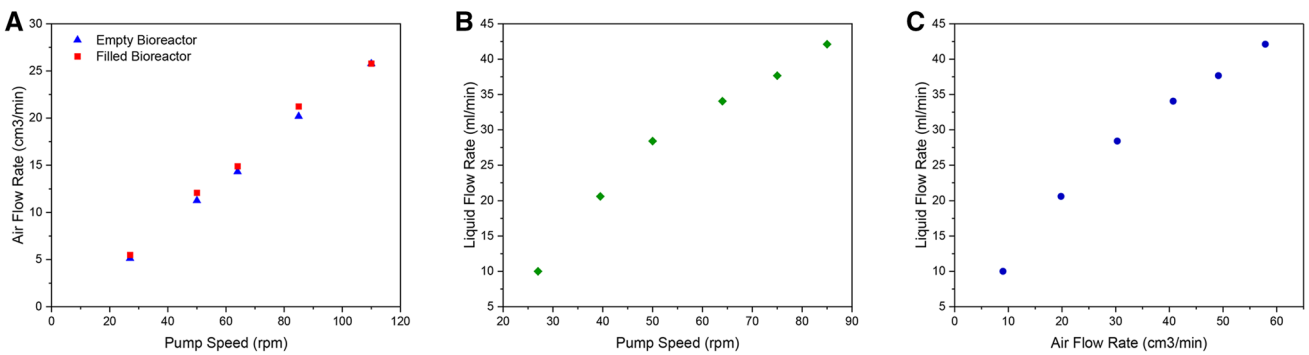

Fig. 5 Fluid dynamics of the EPC. **A** Air flow rate (cm^3/min) as function of the pump speed (RPM). **B** Liquid flow rate (cm^3/min) as function of the pump speed (RPM). **C** Liquid flow rate (cm^3/min) as function of the air flow rate (cm^3/min)

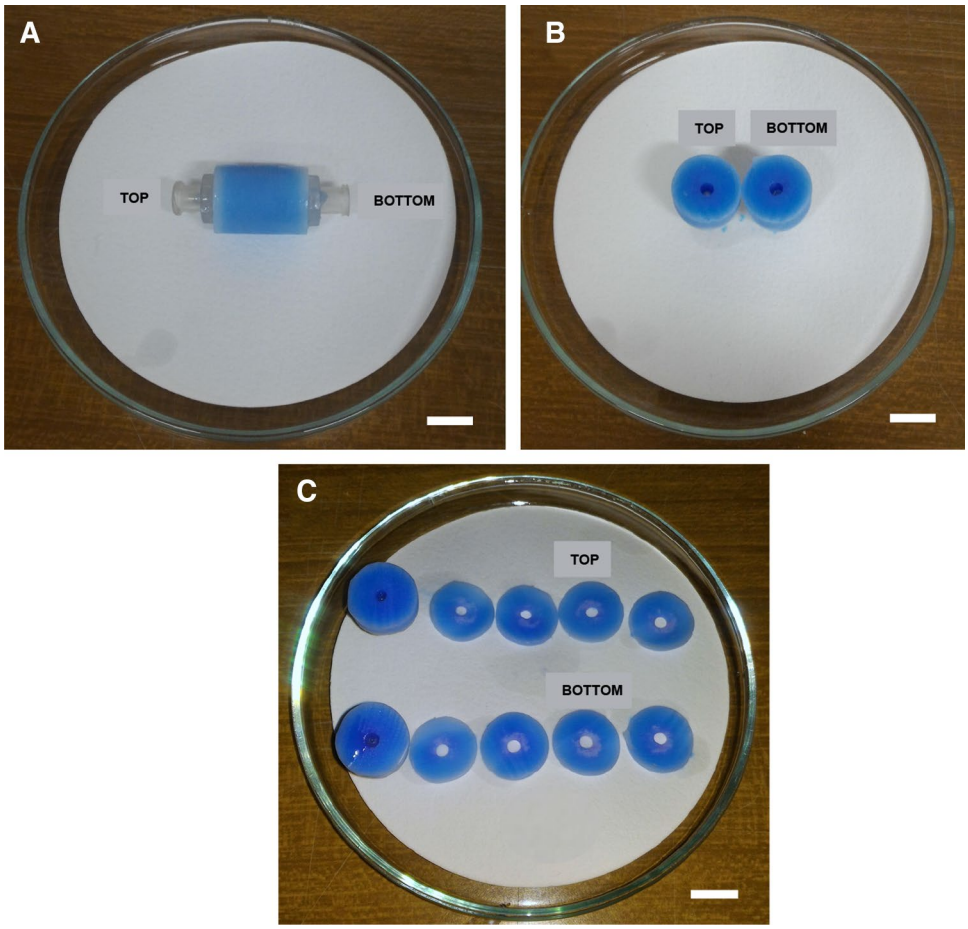

Fig. 6 Real picture of the PLLA scaffold post perfusion inside the dual-flow bioreactor for 40 min using an aqueous solution added with a blue dye: entire scaffold (**A**); top and bottom part of the scaffold (**B**), slices from top and bottom part. Scale bar 1 cm

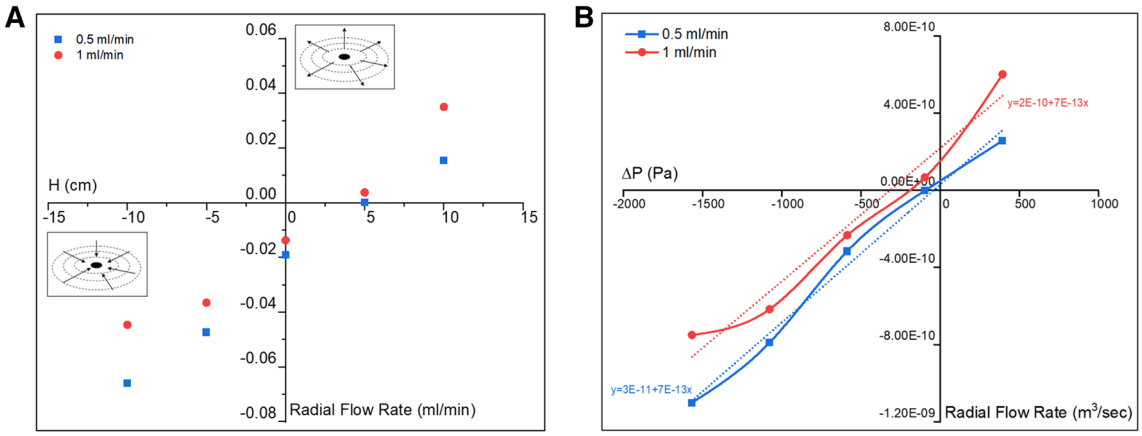

Fig. 7 **A** Radial flow rate (ml/min) through the scaffold as a function of different height levels H (cm) between the bottom of the scaffold and the outlet of IPC tube. **B** Radial Flow Rate (m3/sec) throughout the scaffold as function of the estimated pressure drop ($\Delta P = P_{ext} - P_{int}$) (Pa)

from the edge to the inner channel of the scaffold (in-flow) as a negative flux, whereas a positive sign was adopted for the opposite flow direction (out-flow). For both tested flow rates, when H is negative (i.e., the outlet of the tube is further down with respect the scaffold), a radial flow from the outside toward the inner surface of the scaffold was observed (in-flow). When the outlet of the tube was raised, the flow rate decreased, as long as it turned zero at the level of 5 cm. Raising further, a change of flow direction was observed, since the fluid ran radially from the inner channel to the

outside (out-flow). For both the tested IPC flow rates, the flow increased when increasing *H*.

Evaluation of the scaffold permeability

Starting from the previous results, the absolute permeability of the as-produced scaffold was evaluated, according to the Eq. 2 by combining the permeated flow rates measurements with the Darcy's Theory, Bernoulli's Equation, and Poiseuille's Law. Figure 7 B describes the permeated flow across the scaffold plotted against the estimated total pressure drop, for the two pumped flow rates. Although the linear fitting of the 1 ml/min curve revealed a minor accuracy, still exhibiting a $R^2 > 0.95$, an identical slope resulted for the two fitting lines, thus leading to a constant permeability value. By solving Eq. 2, the calculated permeability *K* was 1.12×10^{-14} m^2.

Preparation and characterization of FNPs

Polymeric FNPs with colloidal size were prepared by following a noted method known as the o/a emulsion-high pressure homogenization (HPH) and by starting from a polymeric pegylated fluorescent derivative of α,β-poly(N-2-hydroxyethyl)-D,L-aspartamide (PHEA). The latter was functionalized in different steps with RhB moieties, PLA and PEG chains at 2,000 molecular weight, to obtain a copolymer which was named PHEA-RhB-PLA-PEG, as described elsewhere [39, 44]. In particular, the synthetic steps were carried out by following the experimental conditions to achieve Derivatization Degrees (DD%) in RhB (DD_{RhB}), in PLA (DD_{PLA}) and in PEG (DD_{PEG}) equal to 0.61 mol%, 4.0 mol% and 12.4 mol%, respectively, which were confirmed by SEC analysis [47]. Once prepared without the use of surfactant or other stabilizing agents thanks to the amphiphilic properties of the copolymer, the FNPs were diluted with a proper NaCl solution to obtain an isotonic aqueous FNPs dispersion at a concentration of 0.1 mg/mL. In these conditions, the particles were characterized in terms of mean number distribution size, polydispersity of distribution and ζ potential using Photon Correlation Spectroscopy (PCS). It was found that these FNPs exhibited colloidal size (224.8 nm, PDI = 0.206) and slightly negative ζ potential (− 2.44 mV).

Distribution of FNPs in the polymeric scaffold

After the evaluation of the perfusion system and the diffusion flow throughout the polymeric scaffold, the efficacy of the radial flow of the apparatus related to the migration of particles inside the scaffold was investigated using the as-prepared FNPs as a potential carrier model. In SEM micrographs (Fig. 8), the FNPs are clearly identifiable within the polymeric structure. As expected, the nanoparticles population is predominant in the lumen surface (Fig. 8A), since it is directly in contact with the circulating flow. A wide population of particles is also evident in the scaffold region near the lumen (Fig. 8B). Then the particles front radially decreases when moving from the central lumen to the external surface (Fig. 8C). These results were confirmed both qualitatively and quantitatively by the analysis of the fluorescence images of the scaffold cross sections (Fig. 9i), where FNPs are marked by the fluorescent dye RhB covalently linked to the polymeric matrix. Under excitation of 530–550 nm, an intense red emission was observed in the area close to the lumen surface with a relatively intensity decreasing up to the external surface (Fig. 9ii). A quantitative analysis using ImageJ software allowed to evaluate the radial nanoparticles distribution after the perfusion process directly referring to their fluorescence signal. As reported in Fig. 9iii, a higher

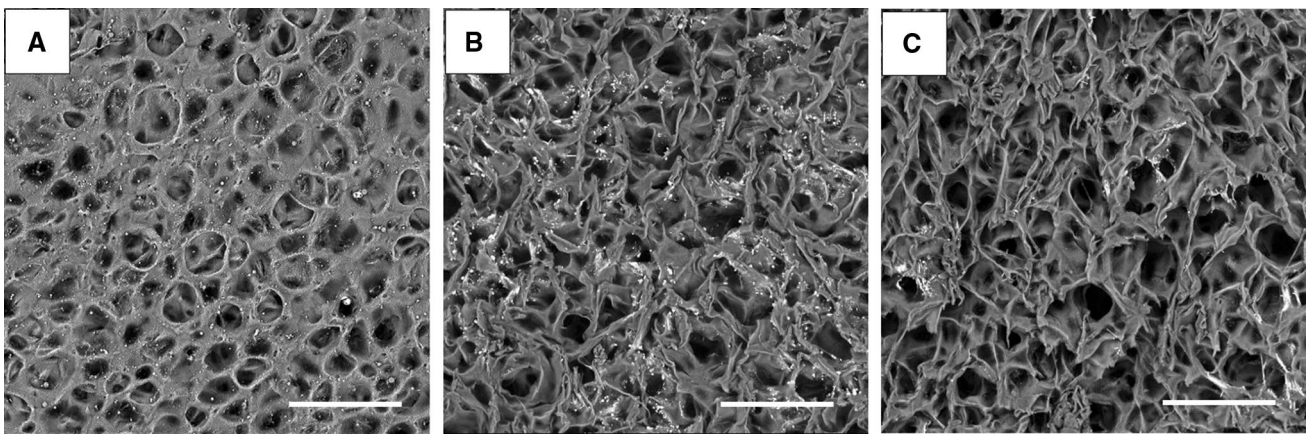

Fig. 8 SEM micrographs of PLLA scaffold cross-sections after the perfusion inside the bioreactor using a solution with FNPs (100 µg/ml): lumen surface (**A**), polymeric matrix close to the lumen (**B**), polymeric matrix portion far from lumen (**C**). Scale bar 80 µm

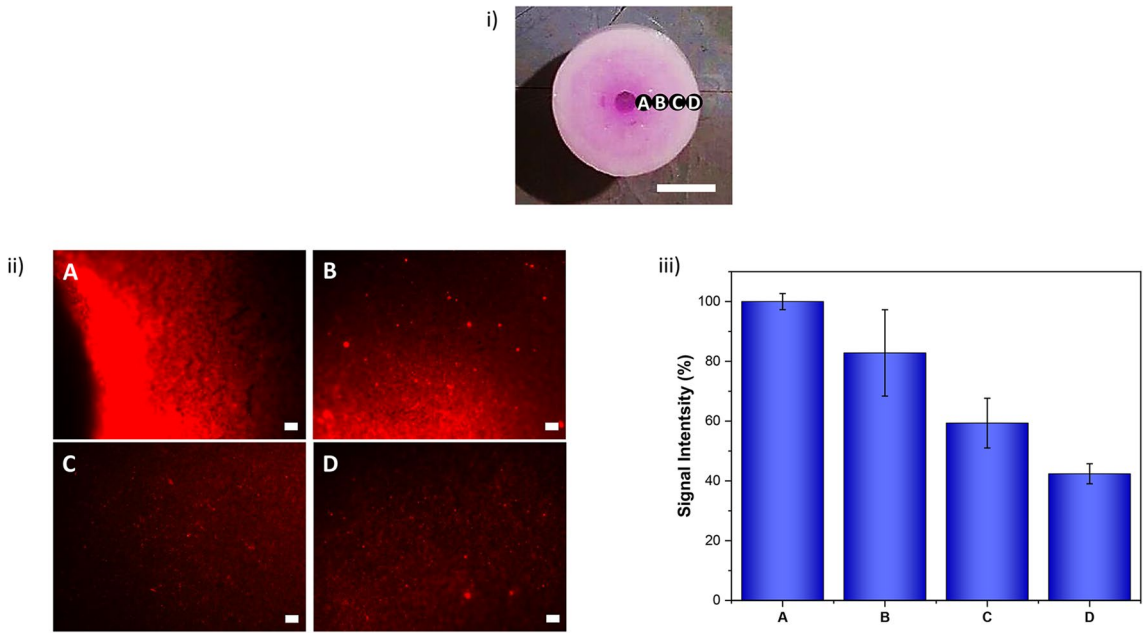

Fig. 9 **i** Real picture of the PLLA scaffold cross section with the 4 areas analyzed: **A** lumen, **B** close to lumen, **C** far from lumen and **D** external surface. Scale bar 1 cm (**ii**) Fluorescence microscopy images of PLLA scaffold cross section after the perfusion of FNPs diffused inside the bioreactor. Scale bar: 50 µm (**iii**) Fluorescence signal intensity (%) of the 4 different areas of the scaffold post perfusion. Data represent mean ± SD. There is no statistically significant different between the samples ($p > 0.05$)

signal intensity was obtained in the region A. The closed region B showed a slight decrement which resulted stronger for the subsequent two region C and D. However, no significant statistically differences were evaluated between the four regions, indicating a uniform diffusion of the FNPs within the polymeric matrix.

Discussion

In the last 20 years, bioreactors have been utilized in several different industry areas [48, 49] and research, especially for the progress of the 3D dynamic cell cultures for human health research [9, 50]. In our work, we presented a custom-made device as an improvement of a common perfusion bioreactor. The goal was to design a perfusion bioreactor with two flow circuits, thus enlarging the traditional use of the bioreactor for TE applications to pharmaceutical purpose, such as the in vitro pre-screening of new drugs. As it is well known, the primary key elements of a bioreactor design are ease of use and assembly [51]. To this end, we developed a compact device easily placeable into a common cell culture incubator. The apparatus, shown in Fig. 10, consists of two perfusion circuits, whose operating principles allow both the radial perfusion through a porous polymeric matrix (IPC circuit) and a continuous circulation of culture medium, at a fixed flow rate, inside the device (EPC circuit) (Fig. 10). Our tests showed that a PLLA scaffold can be fixed at the center of the main column of the IPC while keeping the sterility conditions of the system and avoiding leakage during the liquid circulation. To fabricate porous PLLA scaffolds, many techniques have been reported. Some of these include porogen leaching [52], electrospinning [53], and phase separation [54]. The advantage of using techniques based on Phase Separation to produce scaffolds is the possibility to create an interconnected highly porous micro- or macrostructure [55, 56]. Moreover, phase separation allows to control pore morphology by changing some parameters of the protocol, including polymer concentration, demixing temperature, and time [57]. As a fact, porosity is recognized as one of the crucial parameters for tissue engineering scaffolds [58].

One of the important first steps in developing bioreactors consists of the investigation on engineering parameters, such as fluid profile and hydrodynamic conditions, which can influence the final performance [59, 60]. Operating parameters as liquid flow rates, superficial speeds, pressure drops, and shear stress related to the IPC were analyzed in previous work [42]. In this work, we focused on the analysis and assessment of the EPC fluid dynamics. From our findings, we demonstrated that the device can cover a wide range of liquid flow rates (10–40 ml/min), maintaining both stability of the system and sufficient liquid recirculation.

An interesting result came out from permeability tests which revealed the possibility to manage the direction of the radial flow simply by changing the height of the outlet of the IPC tube. Consequently, according to the desired

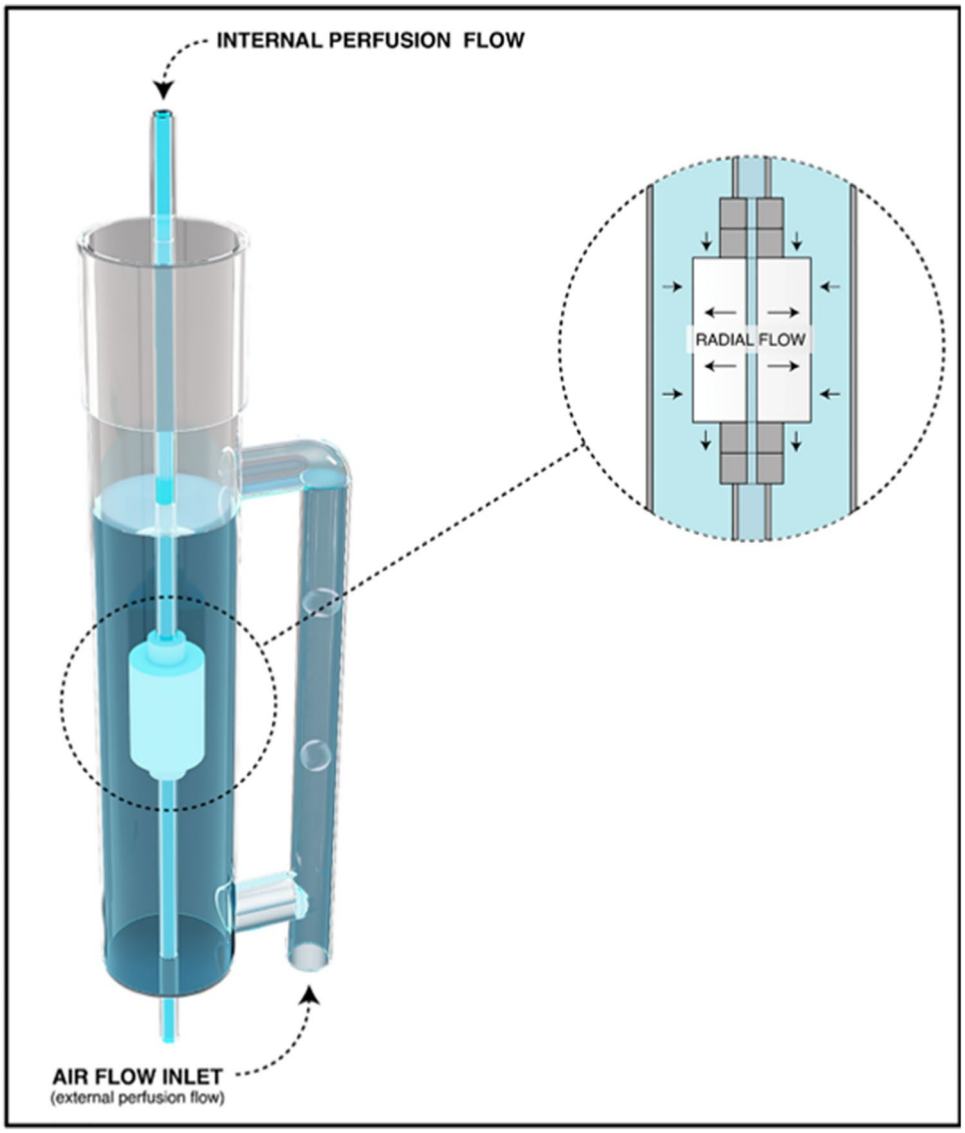

Fig. 10 Illustration of the operating principle of the dual-flow perfusion bioreactor. An internal perfusion flow and an external air perfusion flow generate a "radial flow" throughout the scaffold placed inside the main column of the bioreactor

application, one can precisely set the direction of the radial flow rate, without the use of specific devices [61] or the more approximating results of a computational simulation [62, 63]. Recently, Tan et al. presented a new calibration method for the permeability measuring set-ups by testing the outwards radial flow through two concentric annular slits [64]. In comparison with our outflowing results, this research revealed also an increase of the total pressure drop across the mold at higher flow rates. Although scaffold morphology differs from Tan's tested apparatus, both systems are within the Darcy's flow regime, with an absolute permeability that is independent of the flow rate. Specifically, for our bioreactor, the validity of this assumption was assessed through a semi-empirical method. Our result was perfectly in line with the typical values of permeability to water for TE scaffolds, ranging from 10^{-16} to 10^{-9} m^2 [65]. Similarly, Wang et al. investigated the Darcy permeability of microporous (5–15 µm) PCL scaffold by monitoring fluid flow in response to a range of pressure differentials generated by a Bose Enduratec BioDynamic chamber [66]. From their results, permeability to water of 6×10^{-14} m^2 was measured, matching with our PLLA microporous construct (20–40 µm). Owing to the similar morphological and mechanical properties of PCL and PLLA polymers [54, 67], the agreement between the results of our semi-empirical method and the more accurate measurements of a BioDynamic chamber consolidates the reliability of our protocol. Moreover, we used a low-cost procedure that does not require costly devices, such as pressure transducers [64, 68, 69] and/or dynamic chambers [66].

Generally, the diffusion of macro-, micro- and nanoparticles in porous matrices is fundamental in many biological applications, including drug delivery [70]. Hence, a homogeneous distribution of particles inside a porous support

should be achieved in the devices that simulate the drug delivery process. In the current study, the efficiency of the radial flow was evaluated using polymeric FNPs as potential drug carrier model. PHEA, the biocompatible protein-like copolymer chosen as precursors for the FNPs, shows good water solubility, absence of toxicity, antigenicity and teratogenicity. It has been already successfully utilized as starting material to generate different graft copolymers for several biomedical and pharmaceutical applications [71]. The main reasons for the derivatization reactions in the production steps were the introduction on the polymeric backbone of, respectively: (i) permanently conjugated fluorescent probe moieties (to provide a very high potential to the copolymer in imaging); (ii) biodegradable hydrophobic chains (to obtain an amphiphilic copolymer); (iii) biocompatible chains (to reduce particle aggregation phenomena, to increase the biocompatibility to the resulting copolymer and to confer stealth properties) [38, 72]. A satisfactory level of penetration and an uniform distribution of the particles throughout the entire polymeric matrix, thus demonstrating the potential of our system as an in vitro model for drug pre-screening.

To sum up, according to the data shown above, we can infer that our flow perfusion bioreactor has the ability to generate a good perfusion and an effective radial flow using a wide range of flow rates and low inlet volume. In addition, the highly interconnected porous matrix of the PLLA scaffold certainly promotes the efficacy of the perfusion.

Conclusions

A dual-flow perfusion bioreactor was developed and evaluated as potential system for pre-screening in vitro tests. The dimensions of the apparatus were designed to allow its housing into a standard cell culture incubator and thus reduce the volume of medium that should be sufficient for long term cell cultures. The fluid dynamics properties of the bioreactor were tested and showed that its original design offers several significant advantages over existing bioreactors. First, the device allows a separate control of two perfusion flows through a hollow cylindrical porous scaffold. The external perfusion flow assurances both a good recirculation and oxygenation of the medium, whereas the inner perfusion flow guarantees a radial diffusion through the entire scaffold volume. The direction of this radial flux and the perfusion flow rate can be accurately regulated, according to the desired application. Therefore, the dual-flow design certainly allows maximizing the efficacy of the perfusion dynamic cell culture inside the 3D device. We also showed that the apparatus allows to easily measure the permeability of the scaffold without the use of any pressure sensor that is the most common instrument for this type of evaluation. Finally, the tuneable radial flow from the inner to the outer surface of the scaffold and vice versa demonstrated that our system is able to control migration/diffusion of nanoparticles across a hollow scaffold, while mimicking flow condition suitable for drug release from nano-carriers. Consequently, it can be said that our novel bioreactor has great potential to be used as a versatile device for multiple purposes, including pharmaceutical applications for new therapeutic discoveries.

Acknowledgements The authors kindly acknowledge the master student Valentina Aiello, for her contribution in carrying out the diffusion tests. The authors are grateful to Valerio Spena for providing Fig. 10 (design of the dual-flow bioreactor and its operating principle).

Funding No funding was received for conducting this study.

Declarations

Conflict of interest All the authors declare that they have no commercial or financial conflict of interest.

References

1. Langhans SA (2018) Three-dimensional in vitro cell culture models in drug discovery and drug repositioning. Front Pharmacol 9:1–14. https://doi.org/10.3389/fphar.2018.00006
2. Honek J (2017) Preclinical research in drug development. MEW 26(4):5–8
3. Grainger DW (2014) Cell-based drug testing; this world is not flat. Adv Drug Deliv Rev. https://doi.org/10.1016/j.addr.2014.04.001
4. Rathod CP, Dhawale SC, Kshirsagar RV (2011) Recent trends in screening and evaluation methods of anticancer drugs. Indo Am J Pharm Res 111:506–515
5. Greek R (2013) Animal models in drug development. In: New insights into toxicity and drug testing. Manhattan: InTech 6:124–152. https://doi.org/10.5772/53893
6. Rai J, Kaushik K (2018) Reduction of animal sacrifice in biomedical science & research through alternative design of animal experiments. Saudi Pharm J 26:896–902. https://doi.org/10.1016/j.jsps.2018.03.006
7. Mak IW, Evaniew N, Ghert M (2014) Lost in translation: animal models and clinical trials in cancer treatment. Am J Transl Res 6(2):114–118
8. Sceats E (2010) In vitro tissue models: working in the third dimension. Innov Pharm Technol. https://doi.org/10.1016/j.electacta.2006.09.031
9. Ginai M, Elsby R, Hewitt CJ et al (2013) The use of bioreactors as in vitro models in pharmaceutical research. Drug Discov Today 18:922–935. https://doi.org/10.1016/j.drudis.2013.05.016
10. Brajša K, Trzun M, Zlatar I, Jelić D (2016) Three-dimensional cell cultures as a new tool in drug discovery. Period Biol 118:59–65. https://doi.org/10.18054/pb.2016.118.1.3940
11. Imamura Y, Mukohara T, Shimono Y et al (2015) Comparison of 2D- and 3D-culture models as drug-testing platforms in breast cancer. Oncol Rep 33:1837–1843. https://doi.org/10.3892/or.2015.3767
12. Elliott NT, Yuan F (2011) A review of three-dimensional in vitro tissue models for drug discovery and transport studies. J Pharm Sci 100:59–74. https://doi.org/10.1002/jps.22257

13. Kretlow JD, Klouda L, Mikos AG (2007) Injectable matrices and scaffolds for drug delivery in tissue engineering. Adv Drug Deliv Rev 59:263–273. https://doi.org/10.1016/j.addr.2007.03.013
14. Hume RD, Berry L, Reichelt S et al (2018) An engineered human adipose/collagen model for in vitro breast cancer cell migration studies. Tissue Eng Part A 24:1309–1319. https://doi.org/10.1089/ten.tea.2017.0509
15. Rosellini E, Zhang YS, Migliori B et al (2018) Protein/polysaccharide-based scaffolds mimicking native extracellular matrix for cardiac tissue engineering applications. J Biomed Mater Res Part A 106:769–781. https://doi.org/10.1002/jbm.a.36272
16. Lei C, Zhu H, Li J et al (2015) Preparation and characterization of polyhydroxybutyrate-co- hydroxyvalerate/silk fibroin nanofibrous scaffolds for skin tissue engineering. Acta Med Okayama 70:111–118. https://doi.org/10.1002/pen
17. Nie W, Peng C, Zhou X et al (2017) Three-dimensional porous scaffold by self-assembly of reduced graphene oxide and nano-hydroxyapatite composites for bone tissue engineering. Carbon NY 116:325–337. https://doi.org/10.1016/j.carbon.2017.02.013
18. Schmid J, Schwarz S, Meier-Staude R et al (2018) A perfusion bioreactor-system for cell seeding and oxygen-controlled cultivation of 3D-cell cultures. Tissue Eng Part C Methods. https://doi.org/10.1089/ten.TEC.2018.0204
19. Adcock AF (2015) Three-dimensional (3D) cell cultures in cell-based assays for in-vitro evaluation of anticancer drugs. J Anal Bioanal Tech. https://doi.org/10.4172/2155-9872.1000249
20. Zhao J, Griffin M, Cai J et al (2016) Bioreactors for tissue engineering: an update. Biochem Eng J 109:268–281. https://doi.org/10.1016/j.bej.2016.01.018
21. Adamietz P, Meenen NM, Goepfert C et al (2005) Bioreactor design for tissue engineering. J Biosci Bioeng 100:235–245. https://doi.org/10.1263/jbb.100.235
22. Chen H-C, Hu Y-C (2014) Bioreactors for tissue engineering. Springer Biotechnol Lett. https://doi.org/10.1007/s10529-006-9111-x
23. Spitters TW, Leijten JC, Deus FD, Costa IB, van Apeldoorn AA, van Blitterswijk CA, Karperien M (2013) A dual flow bioreactor with controlled mechanical stimulation for cartilage tissue engineering. Tissue Eng Part C Methods 19(10):774–783
24. Barba AA, Cascone S, Caccavo D et al (2017) Engineering approaches in siRNA delivery. Int J Pharm 525:343–358. https://doi.org/10.1016/j.ijpharm.2017.02.032
25. Melke J, Zhao F, Rietbergen B et al (2018) Localisation of mineralised tissue in a complex spinner flask environment correlates with predicted wall shear stress level localisation. Eur Cells Mater 36:57–68. https://doi.org/10.22203/eCM.v036a05
26. Kabirian F, Amoabediny G, Haghighipour N et al (2015) Nitric oxide secretion by endothelial cells in response to fluid shear stress, aspirin, and temperature. J Biomed Mater Res Part A 103:1231–1237. https://doi.org/10.1002/jbm.a.35233
27. Sailon AM, Allori AC, Davidson EH et al (2009) A novel flow-perfusion bioreactor supports 3D dynamic cell culture. J Biomed Biotechnol. https://doi.org/10.1155/2009/873816
28. Brancoft GN, Sikavitsas VI, Mikos AG (2003) Design of a flow perfusion bioreactor system for bone tissue-engineering. Tissue Eng 9:549–554. https://doi.org/10.1089/107632703322066723
29. Al-Attar T, Madihally SV (2020) Modeling the impact of fluid flow on resveratrol release from electrospun fibers. Comput Biol Med 117:9. https://doi.org/10.1016/j.compbiomed.2020.103622
30. Marrella A, Iafisco M, Adamiano A et al (2018) A combined low-frequency electromagnetic and fluidic stimulation for a controlled drug release from superparamagnetic calcium phosphate nanoparticles: potential application for cardiovascular diseases. J R Soc Interface. https://doi.org/10.1098/rsif.2018.0236
31. Ellis M, Jarman-Smith M, Chaudhuri JB (2005) Bioreactor systems for tissue engineering: a four-dimensional challenge. Bioreact Tissue Eng Princ Des Oper. https://doi.org/10.1007/1-4020-3741-4_1
32. Rizvi SAA, Saleh AM (2018) Applications of nanoparticle systems in drug delivery technology. Saudi Pharm J 26:64–70. https://doi.org/10.1016/j.jsps.2017.10.012
33. Buxton DB (2009) Nanomedicine for the management of lung and blood diseases. Nanomedicine 4:331–339. https://doi.org/10.2217/nnm.09.8
34. Patel T, Zhou J, Piepmeier JM, Saltzman WM (2012) Polymeric nanoparticles for drug delivery to the central nervous system. Adv Drug Deliv Rev 64:701–705. https://doi.org/10.1016/j.addr.2011.12.006
35. Minko T, Rodriguez-Rodriguez L, Pozharov V (2013) Nanotechnology approaches for personalized treatment of multidrug resistant cancers. Adv Drug Deliv Rev 65:1880–1895. https://doi.org/10.1016/j.addr.2013.09.017
36. Afshar M, Dini G, Vaezifar S et al (2020) Preparation and characterization of sodium alginate/polyvinyl alcohol hydrogel containing drug-loaded chitosan nanoparticles as a drug delivery system. J Drug Deliv Sci Technol 56:101530. https://doi.org/10.1016/j.jddst.2020.101530
37. Lombardo ME, Carfì Pavia F, Vitrano I et al (2019) PLLA scaffolds with controlled architecture as potential microenvironment for in vitro tumor model. Tissue Cell 58:33–41. https://doi.org/10.1016/j.tice.2019.04.004
38. Craparo EF, Porsio B, Sardo C et al (2016) Pegylated polyaspartamide–polylactide-based nanoparticles penetrating cystic fibrosis artificial mucus. Biomacromol 17:767–777. https://doi.org/10.1021/acs.biomac.5b01480
39. Craparo EF, Porsio B, Mauro N et al (2015) Polyaspartamide-polylactide graft copolymers with tunable properties for the realization of fluorescent nanoparticles for imaging. Macromol Rapid Commun. https://doi.org/10.1002/marc.201500154
40. Craparo EF, D'Apolito R, Giammona G et al (2017) Margination of fluorescent polylactic acid-polyaspartamide based nanoparticles in microcapillaries in vitro: the effect of hematocrit and pressure. Molecules. https://doi.org/10.3390/molecules22111845
41. Carfì Pavia F, la Carrubba V, Ghersi G, Brucato V (2010) A composite PLLA scaffold for regeneration of complex tissues. Int J Mater Form 3:571–574
42. Carfì Pavia F, La Carrubba V, Ghersi G et al (2017) Double flow bioreactor for in vitro test of drug delivery. Curr Drug Deliv 14:1–8. https://doi.org/10.2174/1567201813666160527141538
43. Shaikh A, Al-Dahhan M (2013) Scale-up of bubble column reactors: a review of current state-of-the-art. Ind Eng Chem Res 52:8091–8108. https://doi.org/10.1021/ie302080m
44. Giammona G, Carlisi B, Palazzo S (1987) Reaction of α, β-poly(N-hydroxyethyl)-DL-aspartamide with derivatives of carboxylic acids. J Polym Sci Part A Polym Chem 25:2813–2818. https://doi.org/10.1002/pola.1987.080251016
45. Craparo EF, Cavallaro G, Bondi ML et al (2006) PEGylated nanoparticles based on a polyaspartamide. Preparation, physicochemical characterization, and intracellular uptake. Biomacromol 7:3083–3092. https://doi.org/10.1021/bm060570c
46. Pourchet L, Petiot E, Loubière C et al (2018) Large 3D bioprinted tissue: heterogeneous perfusion and vascularization. Bioprinting 13:1–7. https://doi.org/10.1016/j.bprint.2018.e00039
47. Porsio B, Craparo EF, Mauro N et al (2018) Mucus and cell-penetrating nanoparticles embedded in nano - into - micro formulations for pulmonary delivery of ivacaftor in patients with cystic fibrosis. ACS Appl Mater Interfaces 10:165–181. https://doi.org/10.1021/acsami.7b14992
48. Nájera-Aguilar HA, Mayorga-Santis R, Gutiérrez-Hernández RF et al (2021) Aged refuse filled bioreactor using like a biological

treatment for sugar mill wastewater. Sugar Tech 23:201–208. https://doi.org/10.1007/s12355-020-00881-4
49. Wang W, Yang Q, Zheng S, Wu D (2013) Anaerobic membrane bioreactor (AnMBR) for bamboo industry wastewater treatment. Bioresour Technol 149:292–300. https://doi.org/10.1016/j.biortech.2013.09.068
50. Jasuja H, Kar S, Katti DR, Katti KS (2021) Perfusion bioreactor enabled fluid-derived shear stress conditions for novel bone metastatic prostate cancer testbed. Biofabrication. https://doi.org/10.1088/1758-5090/abd9d6
51. Stephens JS, Cooper JA, Phelan FR Jr, Dunkers JP (2007) Perfusion flow bioreactor for 3D in situ imaging: investigating cell/biomaterials. Biotechnol Bioeng 97:952–961. https://doi.org/10.1002/bit
52. Pisanti P, Yeatts AB, Cardea S et al (2012) Tubular perfusion system culture of human mesenchymal stem cells on poly- L- lactic acid scaffolds produced using a supercritical carbon dioxide-assisted process. J Biomed Mater Res Part A 100A:2563–2572. https://doi.org/10.1002/jbm.a.34191
53. Liu W, Li Z, Zheng L et al (2016) Electrospun fibrous silk fibroin/poly(L-lactic acid) scaffold for cartilage tissue engineering. Tissue Eng Regen Med 13:516–526. https://doi.org/10.1007/s13770-016-9099-9
54. Díaz E, Puerto I, Sandonis I, Ibañez I (2014) Morphology and mechanical properties of PLLA and PCL scaffolds. Polym Plast Technol Eng 53:150–155. https://doi.org/10.1080/03602559.2013.843699
55. Zhao P, Gu H, Mi H et al (2018) Fabrication of scaffolds in tissue engineering: a review. Front Mech Eng 13:107–119
56. Zeinali R, Del Valle LJ, Torras J, Puiggalí J (2021) Recent progress on biodegradable tissue engineering scaffolds prepared by thermally-induced phase separation (Tips). Int J Mol Sci 22:3504
57. Sultana N, Hassan MI, Lim MM (2015) Composite synthetic scaffolds for tissue engineering and regenerative medicine. Springer, Cham
58. Zhu X, Cui W, Li X, Jin Y (2008) Electrospun fibrous mats with high porosity as potential. Biomacromol 9:1795–1801
59. Mandenius C (2016) Challenges for bioreactor design and operation. In: Bioreactors: Design, Operation and Novel Applications. pp 1–34. https://doi.org/10.1002/9783527683369.ch1
60. Salehi-Nik N, Amoabediny G, Pouran B et al (2013) Engineering parameters in bioreactor's design: a critical aspect in tissue engineering. Biomed Res Int 2013:1–15. https://doi.org/10.1155/2013/762132
61. Egger D, Fischer M, Clementi A et al (2017) Development and characterization of a parallelizable perfusion bioreactor for 3D cell culture. Bioengineering 4:51. https://doi.org/10.3390/bioengineering4020051
62. Nguyen BNB, Ko H, Fisher JP (2016) Tunable osteogenic differentiation of hMPCs in tubular perfusion system bioreactor. Biotechnol Bioeng 113:1805–1813. https://doi.org/10.1002/bit.25929
63. Navarro J, Swayambunathan J, Janes ME et al (2019) Dual-chambered membrane bioreactor for coculture of stratified cell populations. Biotechnol Bioeng 116:3253–3268. https://doi.org/10.1002/bit.27164
64. Tan H, Pillai KM (2009) A method to estimate the accuracy of radial Flowg-based permeability measuring devices. J Compos Mater 43:2307–2332. https://doi.org/10.1177/0021998308102464
65. Pennella F, Cerino G, Massai D et al (2013) A survey of methods for the evaluation of tissue engineering scaffold permeability. Ann Biomed Eng 41:2027–2041. https://doi.org/10.1007/s10439-013-0815-5
66. Wang Y, Tomlins PE, Coombes AGA, Rides M (2010) On the determination of darcy permeability coefficients for a microporous tissue scaffold. Tissue Eng Part C Methods 16:281–289. https://doi.org/10.1089/ten.tec.2009.0116
67. Báez JE, Marcos-Fernández Á (2015) A Comparison of three different biodegradable aliphatic oligoesters (PGA, PLLA, and PCL) with similar linear alkyl end groups by DSC and SAXS. Int J Polym Anal Charact 20:637–644. https://doi.org/10.1080/1023666X.2015.1054138
68. Israelowitz M, Weyand B, Rizvi S et al (2012) Development of a laminar flow bioreactor by computational fluid dynamics. J Healthc Eng 3:455–476. https://doi.org/10.1260/2040-2295.3.3.455
69. Bilodeau K, Couet F, Boccafoschi F, Mantovani D (2005) Thoughts and progress: design of a perfusion bioreactor specific to the regeneration of vascular tissue under mechanical tresses. Artif Organs 29:906–922
70. Stylianopoulos T, Poh MZ, Insin N et al (2010) Diffusion of particles in the extracellular matrix: the effect of repulsive electrostatic interactions. Biophys J 99:1342–1349. https://doi.org/10.1016/j.bpj.2010.06.016
71. Carfì Pavia F, Palumbo FS, La Carrubba V et al (2016) Modulation of physical and biological properties of a composite PLLA and polyaspartamide derivative obtained via thermally induced phase separation (TIPS) technique. Mater Sci Eng C 67:561–569. https://doi.org/10.1016/j.msec.2016.05.040
72. Craparo EF, Licciardi M, Conigliaro A et al (2015) Hepatocyte-targeted fluorescent nanoparticles based on a polyaspartamide for potential theranostic applications. Polymer (Guildf) 70:257–270. https://doi.org/10.1016/j.polymer.2015.06.009